# Prism-shaped Cu nanocatalysts for electrochemical $CO_2$ reduction to ethylene

Hyo Sang Jeon,[†] Sebastian Kunze,[†] Fabian Scholten,[†] and Beatriz Roldan Cuenya*[,†,‡,∥]

[†]Department of Physics, Ruhr-University Bochum, 44780 Bochum, Germany

[‡]Department of Physics, University of Central Florida, 32816 Orlando, USA

[∥]Fritz-Haber-Institut der Max-Planck Gesellschaft, 14195 Berlin, Germany

**ABSTRACT:** Electrochemical $CO_2$ reduction has attracted much attention due to its advantages to convert $CO_2$ gas into useful chemicals and fuels. Herein, we have developed prism-shaped Cu catalysts for efficient and stable $CO_2$ electroreduction by using an electrodeposition method. These Cu prism electrodes were characterized by scanning electron microscopy, X-ray diffraction, and X-ray photoelectron spectroscopy. Electrochemical $CO_2$ reduction measurements show improved activities for $C_2H_4$ production with high partial current density of -11.8 mA/cm², which is over four times higher than that of the planar Cu sample (-2.8 mA/cm²). We have demonstrated that the enhanced $C_2H_4$ production is partially attributed to the higher density of defect sites available on the roughened Cu prism surface. Furthermore, stability tests show a drastic improvement in maintaining $C_2H_4$ production over 12 hours. The enhanced performance and durability of prism Cu catalysts hold promise for future industrial applications.

**KEYWORDS**: $CO_2$ reduction, copper, ethylene, shape effects, defects

The development of sustainable energy sources as alternative to replace the traditional global energy consumption depending on fossil fuels has recently attracted significant attention, since they are not only running out, but causing climate changes due to greenhouse gas $CO_2$ emission during energy production.[1-3] Electrochemical $CO_2$ reduction is a promising process to produce useful fuels with high energy density and can be integrated with various renewable energy such as solar and wind in carbon recycling systems, aiming at closing the artificial energy cycle.[4,5] However, $CO_2$ electroreduction suffers from poor efficiency because much energy is required to reduce $CO_2$ which has a thermodynamically stable structure. Therefore, it is critical to develop efficient electrocatalysts for the structure-sensitive $CO_2$ reduction.

Among the various catalysts for electrochemical $CO_2$ reduction, copper (Cu) has been identified as the most promising catalyst to produce hydrocarbons such as methane ($CH_4$) and ethylene ($C_2H_4$).[6,7] Recently, a number of researchers have focused on the development of highly selective Cu electrocatalysts for $C_2H_4$ production because of its high energy density and its widely use as chemical feedstock in industry.[8-13] Representatively, Hori *et al.* reported that single crystal Cu(100) exhibited high selectivity for $C_2H_4$ production with a Faradaic efficiency (F.E.) of ~ 40% and an even better result of 50% F.E. on Cu(711) at -5 mA/cm² in 0.1 M $KHCO_3$.[13] However, such single crystal Cu substrates are not preferred for commercial applications due to their limitation of scaling up the batch size and high cost. Also, the practical ethylene production rate (*i. e.,* partial current density) of Cu(711) was only -2.5 mA/cm² even though it had 50.0% F.E. of $C_2H_4$. Therefore, it is important to develop new Cu catalysts with higher production rates for the desired products such as $C_2H_4$.

Several studies have suggested that the structure of the Cu surface significantly affects the selectivity of the $CO_2$ reduction products.[14-20] For example, Chen *et al.* reported that Cu mesocrystals synthesized by the in situ reduction of a CuCl film were favorable toward $C_2H_4$ production, where many atomic steps and edges on the Cu mesocrystals surface likely constituted the active sites.[15] Pre-oxidized and subsequently reduced $Cu_2O$ catalysts have also shown high $C_2H_4$ product selectivity, which was initially assumed to be due to grain boundaries that are formed during the successive pre-oxidation and reduction process in the Cu catalysts.[21] The presence of such sites has been proposed to be crucial to enhance the $C_2H_4$ production because it helps to improve the adsorption of C1 intermediates required for the C-C bond formation. This hypothesis has been supported by thermal desorption studies revealing that CO molecules are more strongly absorbed at the surface of pre-oxidized and subsequently reduced $Cu_2O$ catalysts as compared to polycrystalline Cu.[21]

In addition, significant work has been dedicated to the understanding of the various factors affecting the selectivity of the Cu catalysts. The existence of $Cu^+$ species and subsurface oxygen in pre-oxidized Cu catalysts under $CO_2$ electroreduction conditions has been experimentally demonstrated and suggested as an important parameter in the reaction pathway towards $C_2H_4$ and alcohols.[22] Recent theoretical work was in agreement with the previous experimental work and highlighted how the coexistence of $Cu^+/Cu^0$ surface species might favor C-C

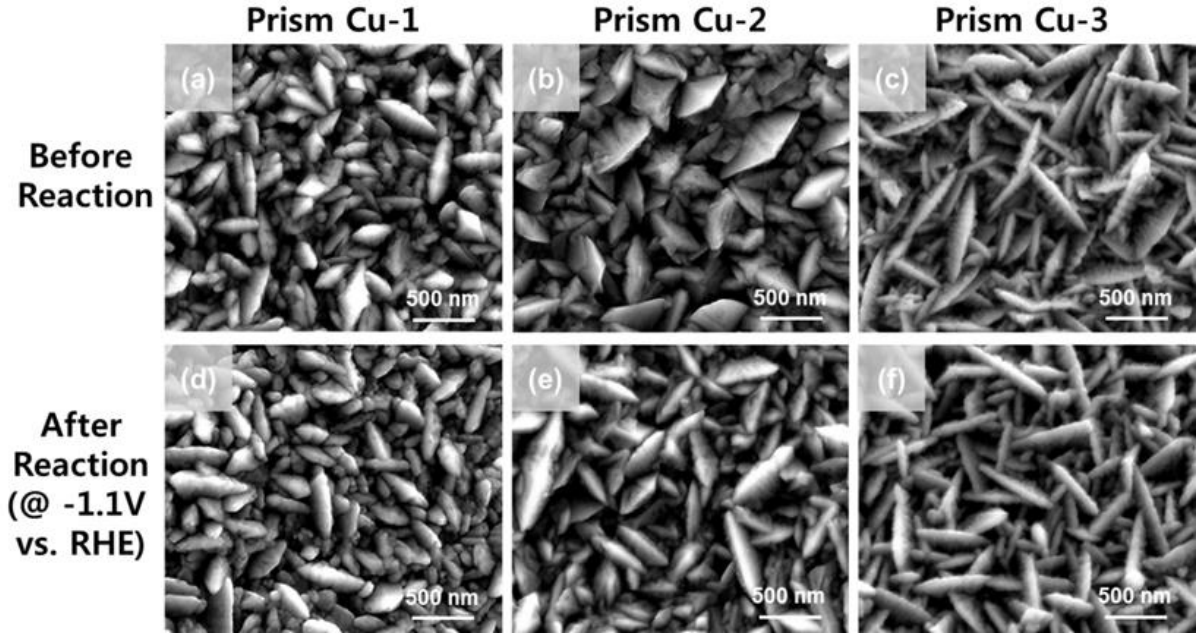


**Figure 1.** SEM images of prism Cu samples (a-c) before and (d-f) after 2 h of electrochemical $CO_2$ reduction at -1.1 V *vs.* RHE.

coupling.[23,24] The use of different electrolytes has also been proposed as another crucial factor determining catalyst selectivity.[25-33] For example, the formation of $C_2H_4$ is favored in an electrolyte with low buffer capacity such as $KClO_4$ and low concentrated $KHCO_3$, which would produce a high local pH near the electrode surface.[25,26] The activity and selectivity of $C_2H_4$ formation is also facilitated in the presence of $Cs^+$ in the bicarbonate solutions[27,28] as well as in halide-containing electrolytes.[29-31] The nanoparticle size has been reported to also affect the selectivity.[32,33] However, while the majority of studies have focused on investigating the former parameters (*i. e.,* grain boundaries, $Cu^+$ species, local pH, and size effects, *etc.*) on $CO_2$ electroreduction activity and selectivity, much less is known about shape effects, and the role of specific crystalline facets.[34-36]

Herein, we have prepared highly defective prism-shaped Cu catalysts using a one-step electrodeposition method. Electrochemical $CO_2$ reduction measurements of prism Cu electrodes have displayed improved activity for $C_2H_4$ production with stable performance for at least 12 hours. We have demonstrated that the presence of a significant fraction of defect sites on the prism Cu surface plays a role in improving $C_2H_4$ production.

The prism-shaped Cu catalysts were prepared in a $Cu^{2+}$ solution including different concentrations of the additives: 0.4 mM (Prism Cu-1), 1.0 mM (Prism Cu-2) and 2.0 mM (Prism Cu-3). Figure 1(a-c) and Figure S1 show the surface morphology of the prism Cu-1, prism Cu-2, and prism Cu-3 samples, respectively. All prism Cu samples display perpendicularly grown triangular nanoprisms with different width of the top and bottom facets, while the planar electropolished Cu reference foil has a flat surface (Figure S2). In addition, the width of the prisms was more uniform and narrow with increasing additive concentration (Janus Green B) and the side edge surface was found to roughen, which is expected to have a higher concentration of defect sites. Our unique structures of prism Cu are caused by the additive effect acting as a crystal modifier and induces the preferential deposition of Cu ions and the formation of the prism shaped morphologies (see Supporting Information).

In order to confirm the crystalline structure of the prism Cu, XRD measurements were carried out (Figure S3). All of the XRD patters were solely associated with the metallic Cu structures (JCPDS 04-0836) without other copper oxide phases such as $Cu_2O$ or CuO. The relative ratio of intensity for (200)/(111) was about 0.3 for all prism Cu samples while planar cu foil was 0.5 (Table S1). This result indicated that the growth of prism Cu is preferred along the (111) plane. In addition, the XPS spectra revealed that there were no residual impurities (*i. e.,* N, S, and Cl) from the sample synthesis (Figure S4).

The potential dependent geometric current densities measured by chronoamperometry were recorded in order to evaluate the electrocatalytic activity of the prism-shaped Cu samples as shown in the Figure 2 and Figure S5. We could confirm that prism Cu samples had higher current density than planar Cu within the entire potential region. At a potential of around -1.1 V *vs.* RHE, the current density of planar Cu, prism Cu-1, prism Cu-2, and prism Cu-3 was -10.3, -17.4, -24.7 and -28.6 mA/cm$^2$, respectively. The three times larger current density value of prism Cu-3 can be partially attributed to the higher surface area of the roughened prism Cu (Figure S6, Table 1). In addition, we could not find any change in the morphology of all catalysts after $CO_2$ electrolysis at -1.1 V *vs.* RHE for 2 hours (Figure 1 (d-f)).

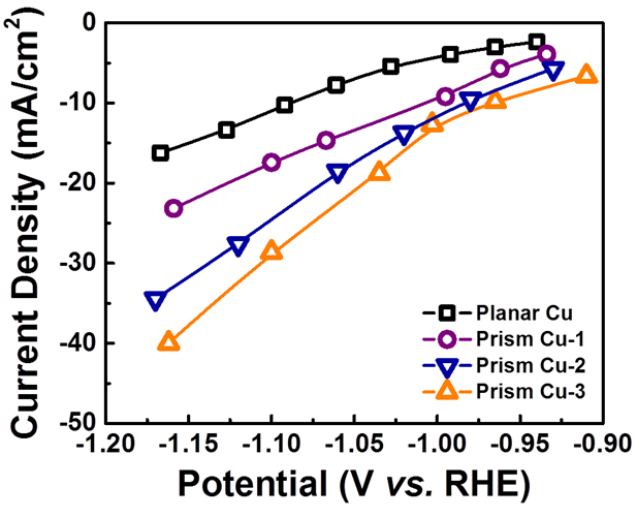


**Figure 2.** Total geometric current densities *vs.* applied potential of a planar Cu foil, prism Cu-1, prism Cu-2, and prism Cu-3.

**Table 1. Values of the electrochemical double layer capacitance and roughness factor. The double layer capacitances were calculated from the slope of the current density *vs.* the scan rate (Figure S6). The roughness factors were obtained by normalizing the capacitance values by that of the planar Cu sample.**

| Sample | Capacitance (uF/cm$^2$) | Roughness Factor |
|---|---|---|
| Planar Cu | 29 | 1.0 |
| Prism Cu-1 | 248 | 8.5 |
| Prism Cu-2 | 365 | 12.6 |
| Prism Cu-3 | 428 | 14.8 |

Figure 3 and Figure S7 show the partial current densities of gas (*i. e.*, $H_2$, CO, $CH_4$, and $C_2H_4$) and liquid (*i. e.*, HCOOH, $C_2H_5OH$, and n-$C_3H_7OH$) products of the $CO_2$ reduction as a function of applied potential, and their F.E. are shown in Figure S8. Although F.E. has important information in the selectivity of $CO_2$ reduction products, the partial current density could be helpful to understand the reaction kinetics of the each of the products.[7,37] The partial current density of $C_2H_4$ of prism Cu-3 was about -11.8 mA/cm$^2$ at -1.16 V *vs.* RHE. This value was about four times higher than that of planar Cu. In contrast to increased $C_2H_4$ production, we could confirm that $CH_4$ partial current density of planar Cu was similar to prism Cu samples. This result indicated that the increase in the $C_2H_4$ production is not simply due to an increase in the surface area of the prism Cu surfaces.

In general, adsorbed *CO (or CHO*) has been known to be a key intermediate for $CH_4$ and $C_2H_4$ formation during $CO_2$ reduction.[38,39] $C_2H_4$ is generated by the dimerization of adsorbed *CO in close proximity to each other followed by hydrogenation, and $CH_4$ is produced by the hydrogenation of adsorbed *CO. According to the previous reports on polycrystalline Cu for $CO_2$ reduction, surface adsorbed C1 intermediates are more favorable to make the $CH_4$ production at very negative potentials, while C-C bond formation is difficult because the probability of reaction between adjacent C1 intermediates be lowered.[7] Interestingly, the $C_2H_4$ partial current density of the prism Cu samples dramatically increases with increasing electrolysis potential, while the planar Cu sample displays a constant production rate over -1.1 V *vs.* RHE. This result indicates that the prism Cu samples have certain crystalline facets that favor the dimerization of adsorbed *CO species without a significant change in other factors involved in the hydrogenation of adsorbed *CO.

The prism Cu samples exhibited greater activity for $H_2$ production than planar Cu, which suggests that the proton that was not participating in the hydrogenation with adsorbed *CO to make methane may be released as hydrogen. The CO partial current density of all the samples appears to be the same, which implies that CO, well-known as an intermediate species, was efficiently used to make hydrocarbons. Lastly, we could observe that the $C_2H_5OH$ and n-$C_3H_7OH$ partial current densities increased in the prism Cu samples, which is thought to be related to the improved $C_2H_4$ formation.[8,40]

We assume that defect sites on the surface of prism Cu samples lead to high $C_2H_4$ productivity. Tang *et al.* reported that Cu nanoparticles with roughened surface showed good selectivity toward $C_2H_4$ formation.[14] They proposed that low-coordination sites on the Cu surface were more likely to enhance $C_2H_4$ formation, since their DFT calculations indicated that C1 intermediates are more stable at stepped sites on the Cu surface. Recently, Ren *et al.* showed that Cu nanocrystals exhibited enhanced activity for n-propanol production from $CO_2$ reduction because numerous defect sites on its surfaces stabilized the $C_2H_4$ intermediates.[40] In particular, through simple cyclic voltammetry measurement, they identified the voltammetric feature for the defect sites by confirming unique reduction peaks on their Cu nanocrystal catalysts which are absent in Cu single-crystal surfaces. Interestingly, they found that the integrated charge values of this peak (*i. e.*, proportional value to the number of defect sites) correlated linearly to the production rate of n-propanol.[40] Our cyclic voltammetry experiments also served to identify the density of the defect sites on the prism Cu samples. We found reduction peaks at ~0 and ~0.25 V *vs.* RHE, which are in good agreement with previous results (Figure 4 and Figure S9).[40] A relatively intense reduction peak was observed in the Cu prism samples, while planar Cu showed weak peak intensity at the same potential region. This result indicates that $C_2H_4$ production of our prism Cu samples is improved by the numerous defects sites on the prism Cu surfaces.

However, even though strong defect-related peaks were observed in our voltammograms, we could not find a direct correlation when comparing the $C_2H_4$ partial current density and the integrated charge values of the defect peak. Therefore, there should be other factors

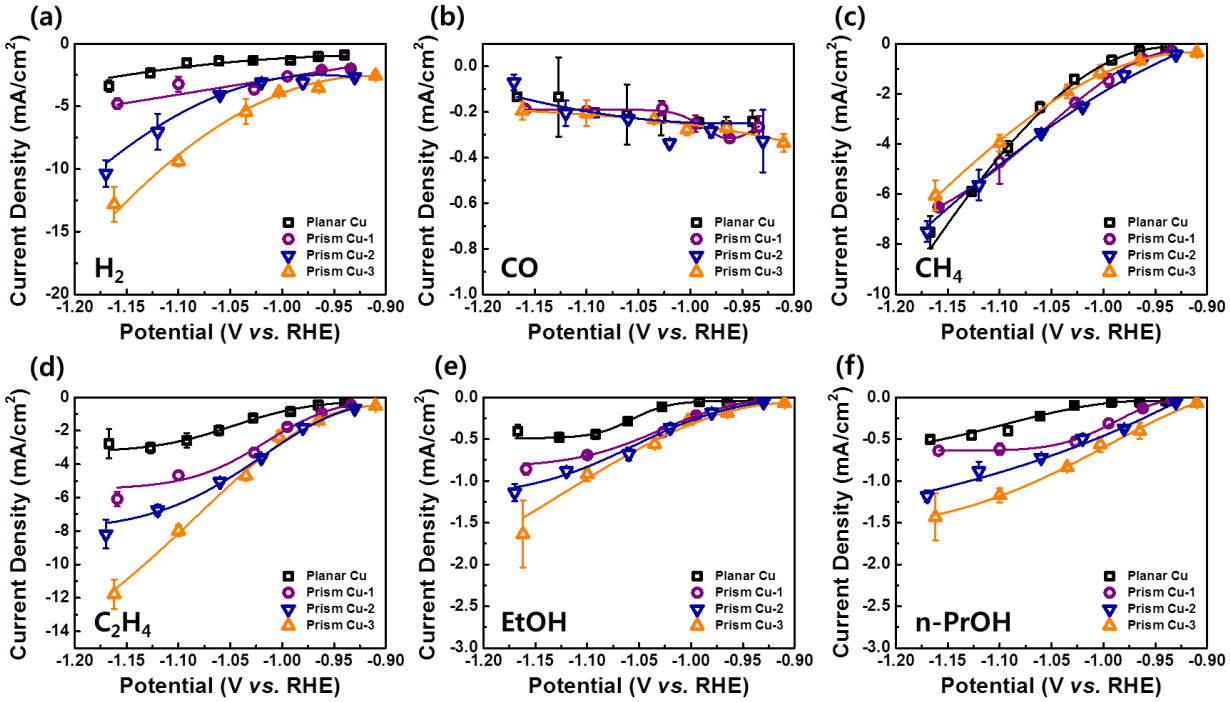


**Figure 3.** Partial current densities *vs.* applied potential for (a) $H_2$, (b) CO, (c) $CH_4$, (d) $C_2H_4$, (e) EtOH, and (f) n-PrOH of a planar Cu foil, prism Cu-1, prism Cu-2, and prism Cu-3.

which are also involved in the increased $C_2H_4$ production of prism Cu. One factor which might contribute to the observed enhanced C2H4 selectivity would be the possible existence of $Cu^+$ species in the catalysts under $CO_2$ reduction reaction conditions, which was observed in pre-oxidized Cu catalysts and assigned to favor C-C coupling.[23,24] To prove the chemical state of prism Cu catalysts during the CO2 reduction reaction, quasi *in situ* XPS measurements were carried out. The prism Cu-3 sample was measured via XPS before and after 2 hour of CO2 electro-reduction at -1.1 V vs. RHE. The Cu Auger

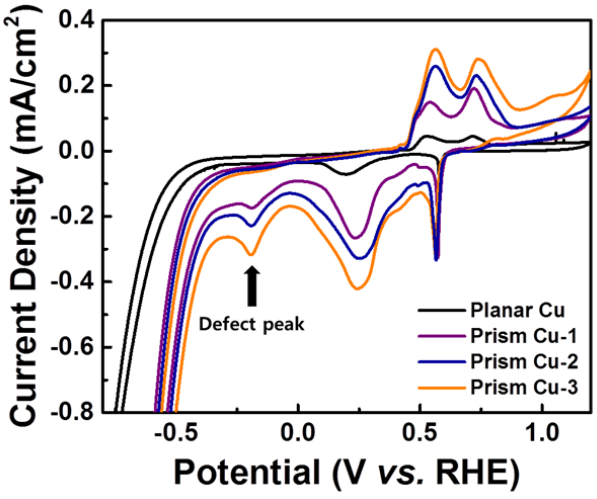


**Figure 4.** Cyclic voltammograms of a planar Cu foil, prism Cu-1, prism Cu-2, and prism Cu-3 in $N_2$-saturated 0.1 M $KHCO_3$ electrolyte.

LMM spectra shown in Figure S10 indicate that the prism Cu-3 sample contained metallic Cu and Cu oxide species before the reaction, formed upon sample exposure to air. However, after the reaction no $Cu^+$ species were detected. This result indicates that the oxidation state of our Cu prism catalysts does not play a role in the observed ethylene selectivity.

Another possible factor is a modification of the local pH, since it has been reported that the reaction pathway of $CO_2$ reduction is preferred toward $C_2H_4$ formation when the local pH increases.[28,41] Thus, it is expected that the increase of the local pH due to high current densities on the highly roughened prism Cu surface could lead to a reaction pathway toward $C_2H_4$ formation. As a result, the enhanced $C_2H_4$ production of the prism Cu samples is postulated to be due to the simultaneous effect of local pH changes and the presence of defect sites.

Lastly, the stability of the prism Cu-3 was investigated at -1.1 V *vs.* RHE for 12 hours (Figure 5). In our setup, a Selemion membrane was installed to separate the cathode and anode part and 0.1 M $KHCO_3$ electrolyte was used after purifying the trace metal ion impurities by using a cation-exchange resin (*i. e.,* Chelex 100 resin).[42,43] The total current density and $C_2H_4$ F.E. were maintained at almost a constant level of ~28.6 mA/cm² and ~27.8%, respectively, which means that $C_2H_4$ gas is consistently produced at a rate of ~24.7 μmol/hr·cm² on our prism Cu electrodes. Interestingly, when we conducted the same stability measurement in the unpurified electrolyte, we could confirm that $C_2H_4$ F.E. dramatically decreased while $H_2$ F.E. increased (Figure S11). This is explained by the

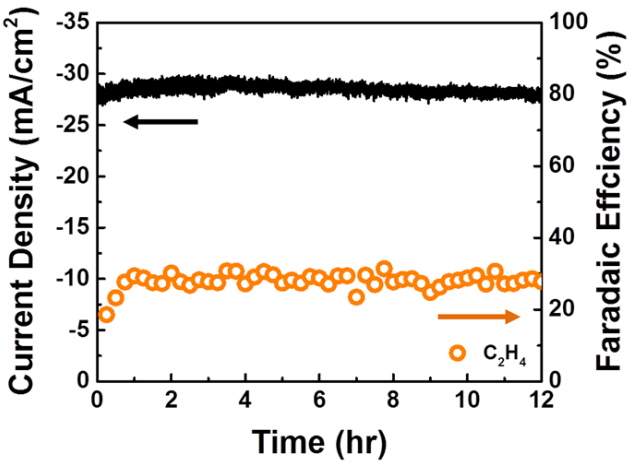


**Figure 5.** Total current density and $C_2H_4$ F.E. of prism Cu-3 at -1.1 V *vs.* RHE for 12 hours.

previous research conducted by Wuttig *et al.* demonstrating that trace amount of metal impurities in the electrolyte were simultaneously deposited on the electrode surface during the $CO_2$ reduction reaction, which resulted in an increase in the $H_2$ evolution reaction over time while suppressing the $CO_2$ reduction reaction.[42] Being able to remove such metal impurities, as was implemented here, is of major importance in order to achieve a prolonged stability during $CO_2$ reduction reactions. Our Cu prisms Cu appear to be promising catalyst candidates due to their simple synthesis, high performance and durability.

In summary, we have prepared prism shaped Cu electrocatalysts by an electrochemical deposition method using crystal modifier additive. The prism Cu samples exhibited high $CO_2$ reduction reaction activity in terms of $C_2H_4$ production and excellent stability over at least 12 hours. It is expected that the enhanced $C_2H_4$ production is attributed to the simultaneous effect of possible changes in the local pH and the presence of low-coordinated atoms at defect sites on the roughened Cu prism surface.

## ASSOCIATED CONTENT

**Supporting Information**.

The Supporting Information is available free of charge on the ACS Publications website at DOI:

Experimental details, additional SEM images, XRD data, XPS data, Faradaic efficiency, and additional analysis of the electrochemical data.

## AUTHOR INFORMATION

### Corresponding Author

* E-mail for B.R.C.: Roldan@fhi-berlin.mpg.de.

### Notes

The authors declare no competing financial interest.

## ACKNOWLEDGMENT

This work was funded by the German Federal Ministry of Education and Research (BMBF) under grants #03SF0523C (CO2EKAT) and 033RCOO4D (eEthylene), the Cluster of Excellence RESOLV at RUB (EXC 1069) funded by the Deutsche Forschungsgemeinschaft, and the ERC OPERANDOCAT (ERC-725915). In addition, financial support was provided by the US National Science Foundation (NSF-CHEM 1213182). The authors acknowledge Xingli Wang (TU Berlin) and Dr. Fernando Rinaldi (Bruker AXS GmbH) for XRD measurements.

## REFERENCES

(1) Turner, J. A. *Science* **1999,** 285, 687-689.
(2) Centi, G.; Quadrelli, E. A.; Perathoner, S. *Energy Environ. Sci.* **2013,** 6, 1711-1731.
(3) Lewis, N. S.; Nocera, D. G. *Proc. Natl. Acad. Sci. U. S. A.* **2006,** 103, 15729-15735.
(4) Whipple, D. T.; Kenis, P. J. A. *J. Phys. Chem. Lett.* **2010,** 1, 3451-3458.
(5) Kondratenko, E. V.; Mul, G.; Baltrusaitis, J.; Larrazabal, G. O.; Perez-Ramirez, *J. Energy Environ. Sci.* **2013,** 6, 3112-3135.
(6) Hori, Y. In Modern Aspects of Electrochemistry; Vayenas, C. G., White, R. E., Gamboa-Aldeco, M. E., Eds.; Springer: New York, **2008;** Vol. 42.
(7) Kuhl, K. P.; Cave, E. R.; Abram, D. N.; Jaramillo, T. F. *Energy Environ. Sci.* **2012,** 5, 7050-7059.
(8) Ren, D.; Deng, Y.; Handoko, A. D.; Chen, C. S.; Malkhandi, S.; Yeo, B. S. *ACS Catal.* **2015,** 5, 2814-2821.
(9) Yano, H.; Tanaka, T.; Nakayama, M.; Ogura, K. *J. Electroanal. Chem.* **2004,** 565, 287-293.
(10) Reller, C.; Krause, R.; Volkova, E.; Schmid, B.; Neubauer, S.; Rucki, A.; Schuster, M.; Schmid, G. *Adv. Energy Mater.* **2017,** 1602114.
(11) Handoko, A. D.; Ong, C. W.; Huang, Y.; Lee, Z. G.; Lin, L.; Panetti, G. B.; Yeo, B. S. *J. Phys. Chem. C* **2016,** 120, 20058-20067.
(12) Engelbrecht, A.; Hämmerle, M.; Moos, R.; Fleischer, M.; Schmid, G. *Electrochim. Acta* **2017,** 224, 642-648.
(13) Hori, Y.; Takahashi, I.; Koga, O.; Hoshi, N. *J. Mol. Catal. A: Chem.* **2003,** 199, 39-47.
(14) Tang, W.; Peterson, A. A.; Varela, A. S.; Jovanov, Z. P.; Bech, L.; Durand, W. J.; Dahl, S.; Norskov, J. K.; Chorkendorff, I. *Phys. Chem. Chem. Phys.* **2012,** 14, 76-81.
(15) Chen, C. S.; Handoko, A. D.; Wan, J. H.; Ma, L.; Ren, D.; Yeo, B. S. *Catal. Sci. Technol.* **2015,** 5, 161-168.
(16) Mistry, H.; Varela, A. S.; Kühl, S.; Strasser, P.; Roldan Cuenya, B. *Nat. Rev. Mater.* **2016,** 1, 16009.
(17) Yang, K. D.; Ko, W. R.; Lee, J. H.; Kim, S. J.; Lee, H.; Lee, M. H.; Nam, K. T. *Angew. Chem., Int. Ed.* **2017,** 56, 796-800.
(18) Lee, S.; Kim, D.; Lee, J. *Angew. Chem., Int. Ed.* **2015,** 54, 14701-14705.
(19) Sen, S.; Liu, D.; Palmore, G. T. R. *ACS Catal.* **2014,** 4, 3091-3095.
(20) Li, C. W.; Kanan, M. W. *J. Am. Chem. Soc.* **2012,** 134, 7231-7234.
(21) Verdaguer-Casadevall, A.; Li, C. W.; Johansson, T. P.; Scott, S. B.; McKeown, J. T.; Kumar, M.; Stephens, I. E. L.; Kanan, M. W.; Chorkendorff, I. *J. Am. Chem. Soc.* **2015,** 137, 9808-9811.
(22) Mistry, H.; Varela, A. S.; Bonifacio, C. S.; Zegkinoglou, I.; Sinev, I.; Choi, Y.-W.; Kisslinger, K.; Stach, E. A.; Yang, J. C.; Strasser, P.; Roldan Cuenya, B. *Nat. Commun.* **2016,** 7, 12123.
(23) Favaro, M.; Xiao, H.; Cheng, T.; Goddard, W. A.; Yano, J.; Crumlin, E. J. *Proc. Natl. Acad. Sci. USA* **2017,** 114, 6706-6711.

(24) Cheng, T.; Xiao, H.; Goddard, W. A. J. *Proc. Natl. Acad. Sci. USA* **2017,** 114, 1795-1800.
(25) Ma, M.; Djanashvili, K.; Smith, W. A. *Angew. Chem.* **2016,** 128, 6792-6796.
(26) Schouten, K. J. P.; Pérez Gallent, E.; Koper, M. T. M. *J. Electroanal. Chem.* **2014,** 716, 53-57.
(27) Murata, A.; Hori, Y. B. *Chem. Soc. Jpn.* **1991,** 64, 123–127.
(28) Singh, M. R.; Kwon, Y.; Lum, Y.; Ager, J. W.; Bell, A. T. *J. Am. Chem. Soc.* **2016,** 138, 13006-13012.
(29) Varela, A. S.; Ju, W.; Reier, T.; Strasser, P. *ACS Catal.* **2016,** 6, 2136–2144.
(30) Ogura, K.; Ferrell, J. R.; Cugini, A. V.; Smotkin, E. S.; Salazar- Villalpando, M. D. *Electrochim. Acta* **2010,** 56, 381–386.
(31) Gao, D.; Scholten, F.; Roldan Cuenya, B. *ACS catal.* **2017,** 7, 5112-5120
(32) Reske, R.; Mistry, H.; Behafarid, F.; Roldan Cuenya, B.; Strasser, P. *J. Am. Chem. Soc.* **2014,** 136, 6978-6986.
(33) Mistry, H.; Reske, R.; Zeng, Z.; Zhao, Z.; Greeley, J.; Strasser, P.; Roldan Cuenya, B. *J. Am. Chem. Soc.* **2014,** 136, 16473-16476.
(34) Loiudice, A.; Lobaccaro, P.; Kamali, E. A.; Thao, T.; Huang, B. H.; Ager, J. W.; Buonsanti, R. *Angew. Chem., Int. Ed.* **2016,** 55, 5789-5792.
(35) Roberts, F. S.; Kuhl, K. P.; Nilsson, A. *Angew. Chem., Int. Ed.* **2015,** 127, 5268-5271.
(36) Gao, D.; Zegkinoglou, I.; Divins, N. J.; Scholten, F.; Sinev, I.; Grosse, P.; Roldan Cuenya, B. *ACS Nano* **2017,** 11, 4825-4831.
(37) Martin, A. J.; Larrazabal, G. O.; Perez-Ramirez, *J. Green Chem.* **2015,** 17, 5114-5130.
(38) Schouten, K. J. P.; Kwon, Y.; van der Ham, C. J. M.; Qin, Z.; Koper, M. T. M. *Chem. Sci.* **2011,** 2, 1902-1909.
(39) Peterson, A. A.; Abild-Pedersen, F.; Studt, F.; Rossmeisl, J.; Norskov, J. K. *Energy Environ. Sci.* **2010,** 3, 1311-1315
(40) Ren, D.; Wong, N. T.; Handoko, A. D.; Huang, Y.; Yeo, B. S. *J. Phys. Chem. Lett.* **2016,** 7, 20-24.
(41) Kas, R.; Kortlever, R.; Yılmaz, H.; Koper, M. T. M.; Mul, G. *ChemElectroChem* **2015,** 2, 354-358.
(42) Wuttig, A.; Surendranath, Y. *ACS Catal.* **2015,** 5, 4479-4484.
(43) Hall, A. S.; Yoon, Y.; Wuttig, A.; Surendranath, Y. *J. Am. Chem. Soc.* **2015,** 137, 14834-14837.

# TOC

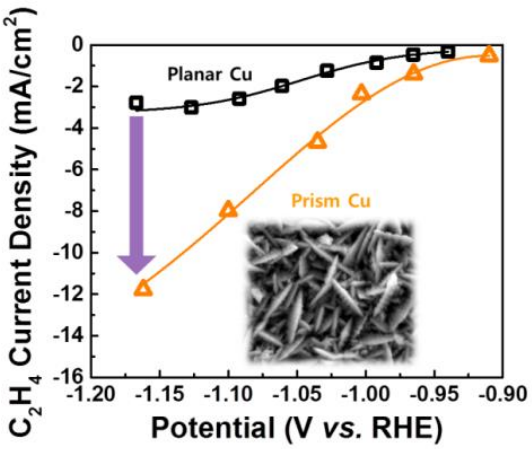
Planar Cu
Prism Cu
$C_2H_4$ Current Density (mA/cm$^2$)
Potential (V *vs.* RHE)
0
-2
-4
-6
-8
-10
-12
-14
-16
-1.20
-1.15
-1.10
-1.05
-1.00
-0.95
-0.90

**Supporting Information**

# Prism-shaped Cu nanocatalysts for electrochemical $CO_2$ reduction to ethylene

Hyo Sang Jeon,[†] Sebastian Kunze,[†] Fabian Scholten,[†] and Beatriz Roldan Cuenya*[,†,‡,ǁ]

[†]Department of Physics, Ruhr-University Bochum, 44780 Bochum, Germany

[‡]Department of Physics, University of Central Florida, 32816 Orlando, USA

[ǁ]Fritz-Haber-Institut der Max-Planck Gesellschaft, 14195 Berlin, Germany

* Corresponding author. Roldan@fhi-berlin.mpg.de

## Experimental

### Preparation of prism-shaped Cu electrodes.

The prism shaped Cu electrodes were prepared by an electrodeposition method.[S1,S2] Cu foils (Advent Research Materials Ltd., 99.995%) were initially electropolished in 85% phosphoric acid at 3 V versus a titanium foil for 5 min, then thoroughly rinsed with ultrapure water (18.2 MΩ) and dried with nitrogen. The electrodeposition solution was prepared by dissolving 0.25 M $CuSO_4 \cdot 5H_2O$ (99.0-100.5%, Sigma-Aldrich) and 0.3 M $H_3BO_3$ (99.97%, Sigma-Aldrich) in ultrapure water, followed by adding Janus Green B (JGB, Sigma-Aldrich) as an additive to control the prism shaped morphology. Two electropolished Cu foils as working and counter electrode were used in a two electrode configuration. In order to prevent unintended deposition, substrates were covered with a perforated electrical tape with a 7 mm diameter which acted as mask determining the size of the resulting Cu nanoprism sample. The geometric area of the electrodes was 0.385 $cm^2$. A copper wire with an alligator clip was attached to hold the Cu foil electrodes and two Cu foils were used as working and counter electrode, placed facing each other. The electrodes were formed in the electrodeposition solution with an applied current density of -6 $mA/cm^2$ for 3 min. The electrodeposition was performed without stirring. The surface was then generously rinsed in ultrapure water before the electrochemical measurements.

### Electrochemical measurements.

Electrochemical $CO_2$ reduction experiments were conducted using an Autolab potentiostat (Multi Autolab M204) in a two compartment electrochemical cell made of polyether ether ketone (PEEK) separated by an anion-exchange membrane (Selemion AMV) or cation-exchange membrane (Nafion 115). The selemion membrane was used for the long term stability tests. A platinum mesh counter electrode and a leak-free Ag/AgCl reference electrode (Innovative Instruments) were used in a three electrode configuration. Purified 0.1 M $KHCO_3$ solutions were prepared by treating the electrolyte with regenerated Chelex 100 Resin (Bio-Rad) using a procedure reported in Refs.[S3,S4] 0.1 M $KHCO_3$ (99.9%, Sigma-Aldrich) electrolyte was saturated with $CO_2$ till a pH of

6.8 was achieved. A freshly prepared sample was measured with a chronoamperometric technique for 2 hours with respect to each fixed potential. All potential values were converted in terms of the reversible hydrogen electrode (RHE) and corrected for *iR* drop as determined by current interrupt.

Roughness factors were obtained to determine the electrochemical surface area of the electrodes by measuring the double-layer capacitance in a 0.1 M $HClO_4$ solution. The defect sites were identified by measuring the cyclic voltammetry in $N_2$-saturated 0.1 M $KHCO_3$ electrolyte.[S5]

**Growth mechanism of prism Cu.**

Wang *et al.* reported the formation of similarly-shaped cobalt nanocatalysts synthesized by electrodeposition with ethylenediamine as a crystalline modifier and discussed their growth mechanism by using a metal ion deficient layer theory (MIDL).[S1] At the initial stage of the deposition, the MIDL is formed since metal ions are consumed when they are deposited on the substrate. The latter results in metal ions that are vertically deposited in a tip shape while leaving spaces between tips which emerge as a nanocone shape. In the next stage, the deposition path of metal ions is disturbed because an electropositive amine group in the modifier occupies the deposition sites near the tip, resulting in a decrease of the growth in the tip direction. On the other hand, the deposition path is accelerated toward spaces between tips because the electropositive modifier pushes the extra metal ions toward the MIDL region. As a result, the nanocone shape grows similar to our prism Cu. Thus, it seems that our unique structures of prism Cu is obtained due to the additive effect acting as a crystal modifier in a similar growth mechanism described as the one described above.

**Product analysis for $CO_2$ reduction reaction.**

The gas products (*i. e.,* $H_2$, CO, $CH_4$, and $C_2H_4$) were quantified by gas chromatography (GC, Agilent 7890B) equipped with a thermal conductivity detector (TCD) and flame ionization detector (FID). The GC was directly connected to the electrochemical cell for online analysis and gaseous samples were injected by a six-port valve. Each compartment of the electrochemical cell contained 38 mL of electrolyte and

34 mL of headspace, and $CO_2$ gas was bubbled through the electrolyte at an average rate of 20 mL $min^{-1}$. Formate concentration was analyzed by high performance liquid chromatograph (HPLC, Shimadzu Prominence) equipped with a NUCLEOGEL® SUGAR 810 column and refractive index detector (RID). Alcohol concentration (*i. e.,* ethanol, and n-propanol) were analyzed by liquid GC (Shimadzu 2010 plus), equipped with fused silica capillary column and FID.

**Calculations of the partial current and Faradaic efficiency of gas products.**

The partial current and Faradaic efficiencies of each product were calculated from the areas of the GC chromatogram as indicated below:

$$i_{partial} = \text{V} \times \text{flow rate} \times \frac{nFp_0}{RT_0} \quad (1)$$

$$F.\,E. = \frac{i_{partial}}{i_{total}} \times 100 \quad (2)$$

Where V is the volume concentration of gas products based on a previous calibration of the GC, and the flow rate (mL $min^{-1}$) was measured by a universal flow meter (ADM 2000, Agilent Technologies) at the exit of the electrochemical cell. $n$ is the number of transferred electrons for certain product, $i_{total}$ (mA) is a steady-state current, $F$ = 96 485 A s $mol^{-1}$, $p_0$ = 1.013 bar, $T_0$ = 273.15 K, and $R$ = 8.314 J $mol^{-1}$ $K^{-1}$.

**Calculations of the partial current and Faradaic efficiency of liquid products.**

The Faradaic efficiencies and partial current of each product were calculated from the areas of the HPLC or liquid GC chromatogram as indicated below:

$$i_{partial} = \frac{C_{liquid} \times V \times n \times F}{t} \quad (1)$$

$$F.\,E. = \frac{i_{partial}}{i_{total}} \times 100 \quad (2)$$

Where $C_{liquid}$ (mol $L^{-1}$) is the concentration of liquid products based on a previous

calibration of the HPLC and liquid GC, $V$ (L) is the volume of the electrolyte. $n$ is number of transferred electrons for certain product, $t$ (s) is the electrolysis time, $i_{total}$ (mA) is a steady-state current, $F$ = 96 485 A s mol$^{-1}$.

**Characterization.**

The surface morphologies were investigated by a scanning electron microscope (Quanta 200 FEG) from FEI with a field emitter as electron source. The grazing incidence X-ray diffraction (GI-XRD, Bruker D8 Advance) was used to characterize the crystal structure. The quasi *in situ* X-ray photoelectron spectroscopy (XPS) measurements were performed in an ultrahigh-vacuum setup equipped with a nonmonochromatic Al K$\alpha$ X-ray source ($h\nu$ = 1486.6 eV) and a hemispherical electron analyzer (Phoibos 100, SPECS GMbH). The XPS analysis chamber is connected to an *in situ* electrochemical cell. The sample transfer from the electrochemical cell to the XPS UHV chamber is performed in vacuum.

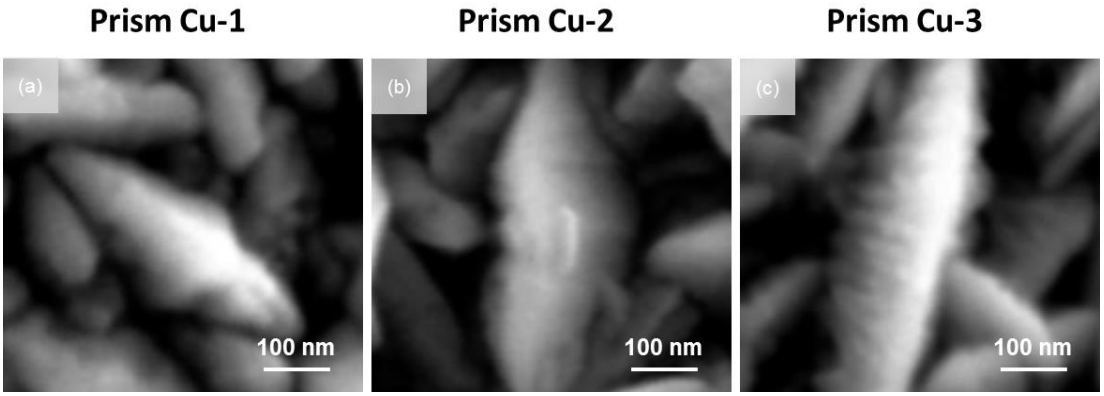


**Figure S1.** High magnification SEM images of prism Cu samples.

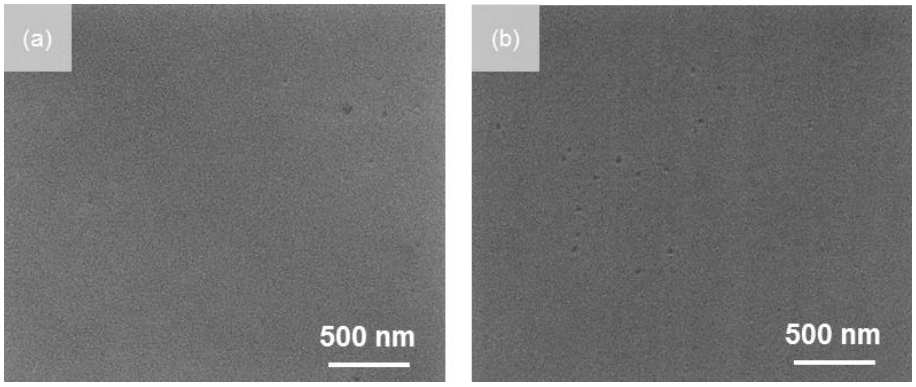


**Figure S2.** SEM images of a planar Cu foil (a) before and (b) after 2 h of electrochemical $CO_2$ reduction at -1.1 V *vs.* RHE.

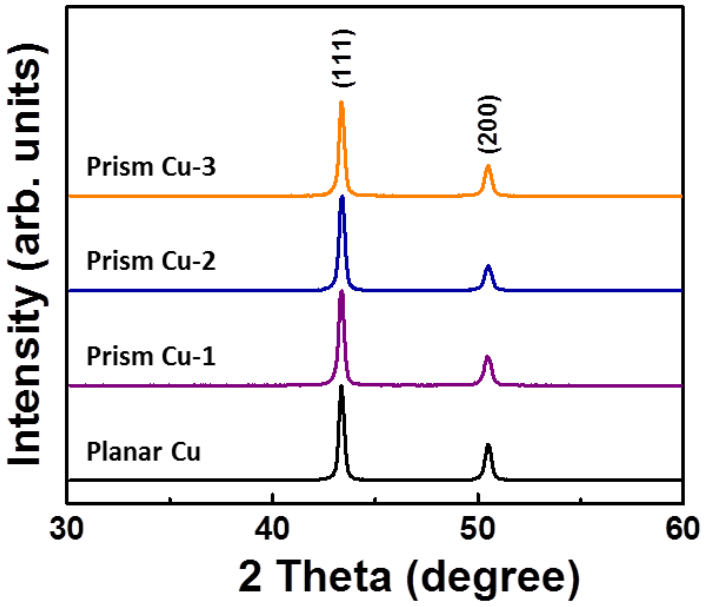


**Figure S3.** XRD diffractograms of a planar Cu foil, prism Cu-1, prism Cu-2, and prism Cu-3 samples. The data were acquired with an incident angle of 2°.

**Table S1.** Intensity ratio of (200)/(111) facet of a planar Cu foil, prism Cu-1, prism Cu-2, and prism Cu-3 samples.

| Samples | Ratio of (200)/(111) |
|---|---|
| Planar Cu | 0.46 |
| Prism Cu-1 | 0.31 |
| Prism Cu-2 | 0.29 |
| Prism Cu-3 | 0.32 |

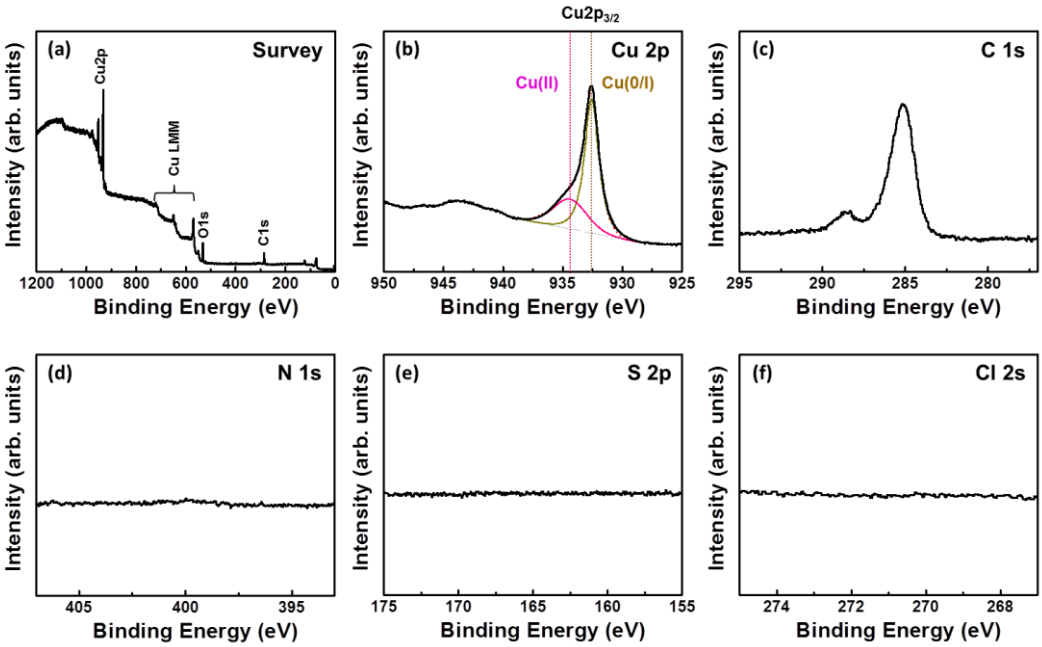


**Figure S4.** XPS spectrum of prism Cu-3 sample. (a) XPS survey spectrum and high-resolution XPS spectra of the following core-level regions: (b) Cu 2p, (c) C 1s, (d) N 1s, (e) S 2p, and (f) Cl 2s, respectively.

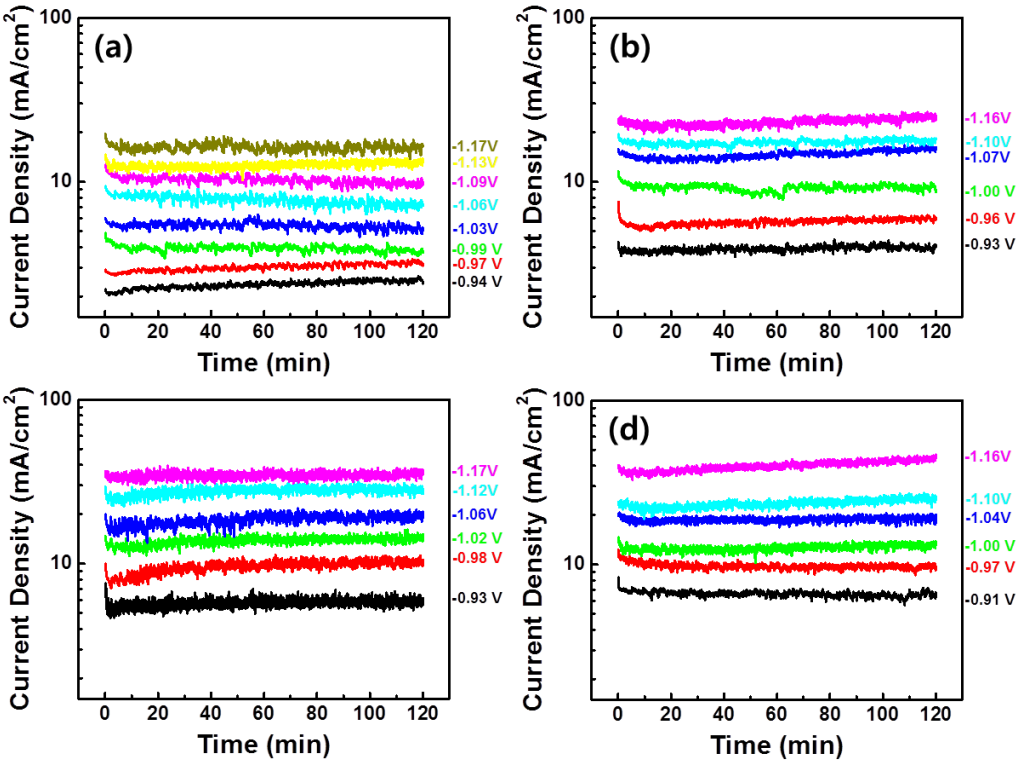


**Figure S5.** Chronoamperometry measurements for $CO_2$ electroreduction of (a) a planar Cu foil, (b) prism Cu-1, (c) prism Cu-2, and (d) prism Cu-3 at various applied potential *vs.* RHE.

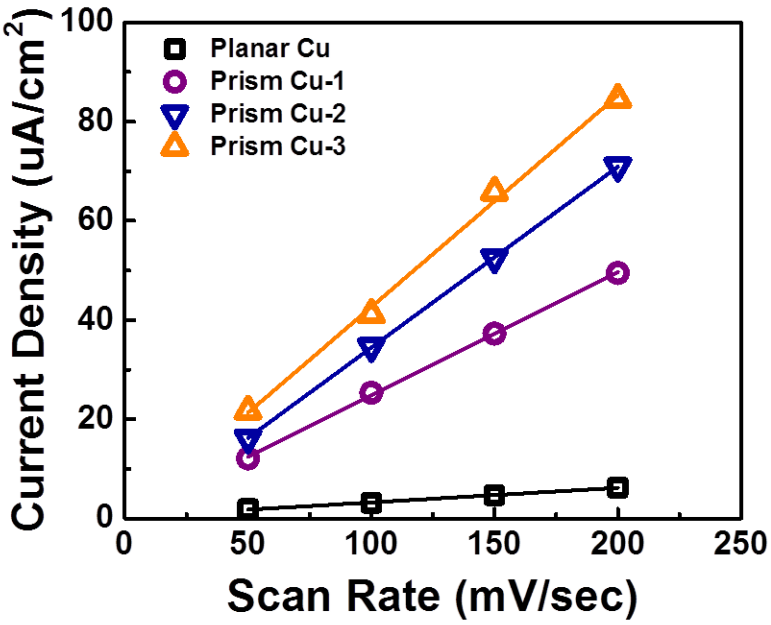


**Figure S6.** Double layer capacitance measurements by cyclic voltammetry of a planar Cu foil, prism Cu-1, prism Cu-2, and prism Cu-3 samples used to extract the roughness factors included in Table 1.

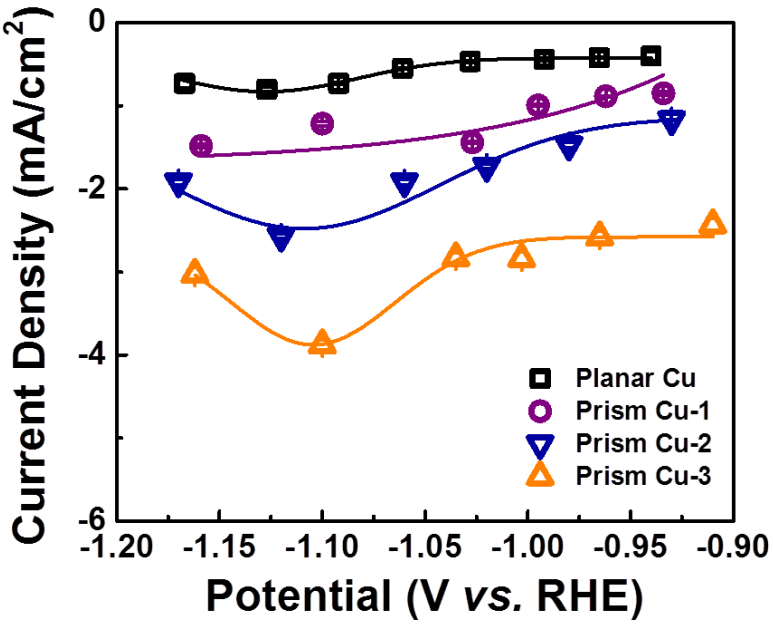


**Figure S7.** Partial current densities *vs.* applied potential for HCOOH production of a planar Cu foil, prism Cu-1, prism Cu-2, and prism Cu-3 samples.

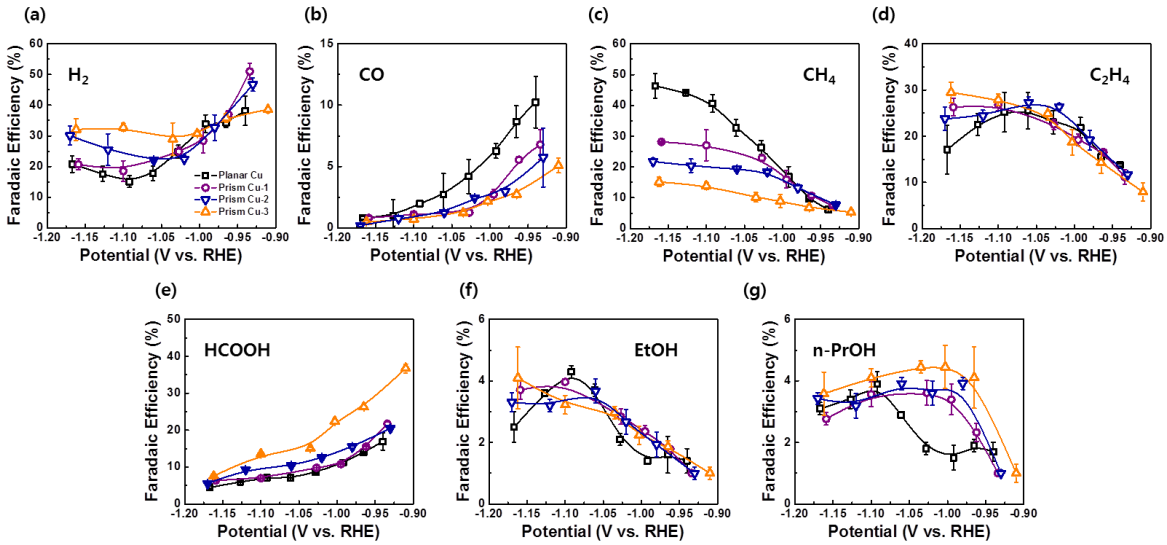


**Figure S8.** Faradaic efficiency *vs.* applied potential for (a) $H_2$, (b) CO, (c) $CH_4$, and (d) $C_2H_4$, (e) HCOOH, (f) EtOH, (g) n-PrOH of a planar Cu foil, prism Cu-1, prism Cu-2, and prism Cu-3 samples. The data were obtained after 2 h of $CO_2$ electroreduction.

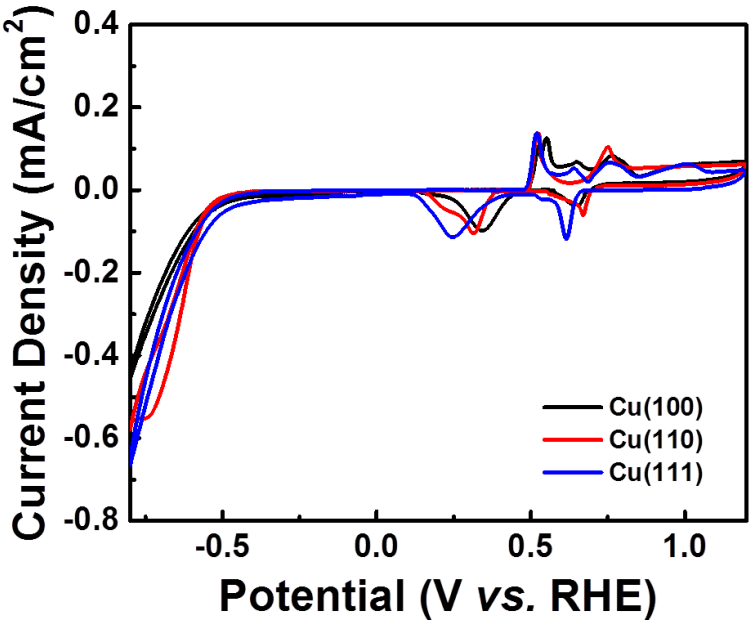


**Figure S9.** Cyclic voltammograms of Cu single-crystals with different orientations in a $N_2$-saturated 0.1 M $KHCO_3$ electrolyte. The defect related peaks observed in prism Cu samples (Figure 4) didn't exhibit in Cu single-crystals, which result means that the voltammetric feature for the defect sites is not caused by specific crystal orientation.

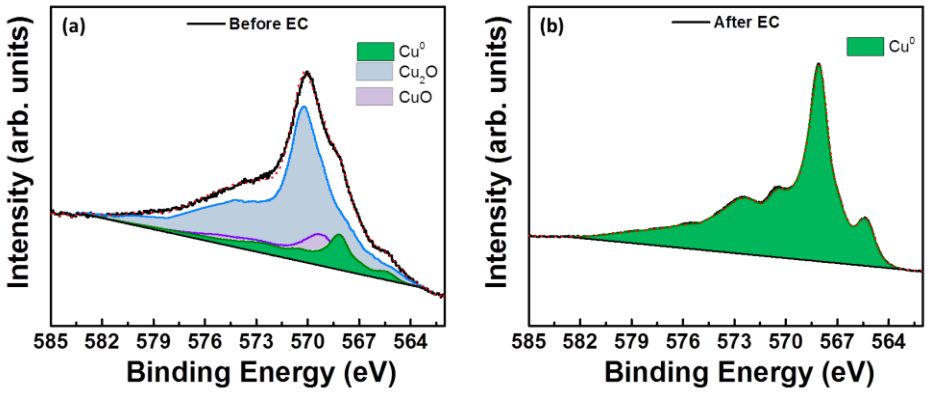


**Figure S10.** Cu Auger LMM XPS spectra of prism Cu-3 sample, measured quasi in situ in a UHV system equipped with an electrochemical cell for in situ sample transfer. The data were acquired (a) before and (b) after 2 h of $CO_2$ electroreduction reaction at -1.1 *vs.* RHE

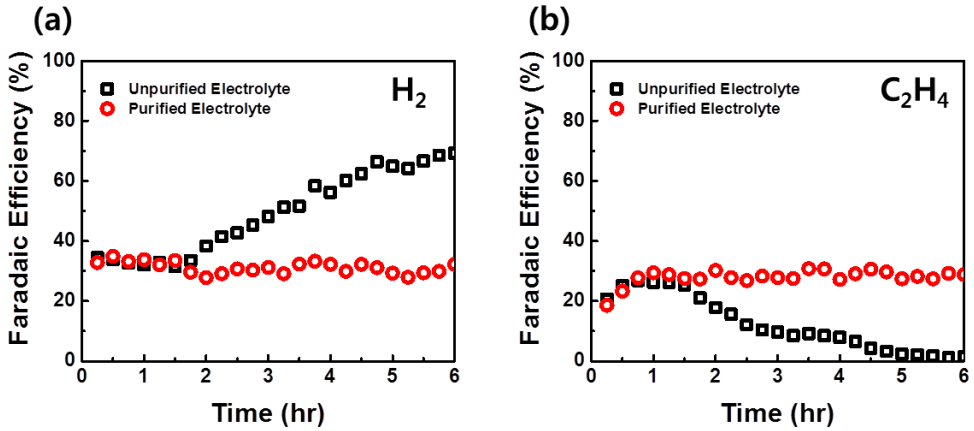


**Figure S11.** Faradaic efficiency of (a) $H_2$ and (b) $C_2H_4$ on the prism Cu-3 in unpurified (black square) and purified (red circle) 0.1 M $KHCO_3$ electrolyte. The measurements were performed with a Selemion membrane and the purified electrolyte was prepared by using a Chelex 100 resin. The importance of the purification in order to remove metal ion residues that strongly affect the reaction selectivity is illustrated.

**References:**

(S1) Wang, H.; Hu, A.; Li, M. CrystEngComm **2014,** 16, 8015-8019.
(S2) Deng, Y.; Ling, H.; Feng, X.; Hang, T.; Li, M. *CrystEngComm* **2015,** 17, 868-876.
(S3) Wuttig, A.; Surendranath, Y. *ACS Catal.* **2015,** 5, 4479-4484.
(S4) Hall, A. S.; Yoon, Y.; Wuttig, A.; Surendranath, Y. *J. Am. Chem. Soc.* **2015,** 137, 14834-14837.
(S5) Ren, D.; Wong, N. T.; Handoko, A. D.; Huang, Y.; Yeo, B. S. *J. Phys. Chem. Lett.* **2016,** 7, 20-24.